

1 Time-lapse camera observations enable fine-grained
2 detection and prediction of alpine vegetation change
3 under earlier snowmelt

4 Ryotaro Okamoto^a, Hiroyuki Oguma^a, Reiko Ide^b

^aBiodiversity Division, National Institute for Environmental Studies,

^bEarth System Division, National Institute for Environmental Studies,

5 **Abstract**

Alpine ecosystems are highly vulnerable to climate change, yet tools for detecting and predicting fine-scale vegetation change remain limited. In the northern Japanese Alps, dwarf bamboo (*Sasa* spp.) is expanding rapidly and threatens alpine plant diversity. Here, we integrated ground-based time-lapse cameras with habitat suitability models (HSMs) to quantify past and future *Sasa* expansion at 1 m spatial resolution. Using time-lapse images collected from 2012 to 2021, we generated automated vegetation classification maps and estimated pixel-level snowmelt timing. Comparison between 2012 and 2021 showed a 48% increase in *Sasa* cover. On average, snowmelt timing advanced by 8.6 days over the past decade. Variable-importance analysis of HSMs identified distance from the prior *Sasa* distribution and the snowmelt day of year (DOY) as the strongest predictors. Under continued advancement of snowmelt, projections indicate further *Sasa* expansion by 2030. This study demonstrates that high-frequency, high-resolution time-lapse imagery combined with HSMs can predict vegetation change with fine spatial detail. The framework offers actionable guidance for conservation, including prioritizing areas for *Sasa* cutting and selecting monitoring sites. The approach is generalizable to other invasive species, providing a scalable tool to assess climate impacts and inform biodiversity conservation in vulnerable alpine ecosystems.

6 **Keywords:** alpine vegetation, habitat suitability modeling, climate change

*Corresponding author

Email addresses: okamoto.ryotaro@nies.go.jp (Ryotaro Okamoto), oguma@nies.go.jp (Hiroyuki Oguma), ide.reiko@nies.go.jp (Reiko Ide)

7

1. Introduction

8 Alpine ecosystems are among the most vulnerable to climate change (Hock
9 et al. (2019)). Numerous studies have documented vegetation shifts in these
10 environments (Gottfried et al. (2012)), including changes in timberline positions
11 and alpine vegetation distributions. These shifts vary across regions, driven by
12 complex interactions between geological and biological factors (Grabherr et al.
13 (2010), Klanderud (2005)).

14 A major driver of vegetation change is the presence of competitively dominant
15 species, which can accelerate community shifts by outcompeting other plants. For
16 instance, grass communities in snowbeds (Grabherr (2003)) and shrub communi-
17 ties in alpine grasslands (Dullinger et al. (2003)) strongly influence surrounding
18 species. In Japanese alpine ecosystems, dwarf bamboo (*Sasa* spp., hereafter
19 *Sasa*) exemplifies such dominance, expanding vigorously and often excluding rare
20 alpine plants. Kudo et al. (2011) demonstrated that earlier snowmelt associated
21 with climate change promotes *Sasa* invasion into snowbed communities, reducing
22 plant species richness by 75%. Conversely, vegetation recovery following *Sasa*
23 removal has been documented (Kudo et al. (2017)), emphasizing the importance
24 of high-resolution monitoring and predictive modeling of *Sasa* expansion for
25 conservation management.

26 Because alpine regions are remote and topographically rugged, traditional
27 vegetation surveys are often costly and logistically demanding. Moreover, fre-
28 quent cloud cover and the complex, mosaic-like structure of alpine vegetation
29 make satellite-based observations particularly challenging. To address these
30 challenges, we previously developed a method for generating high-resolution
31 vegetation classification maps using ground-based time-lapse cameras (Okamoto
32 et al. (2024)). This method utilizes temporal changes in vegetation color cap-
33 tured by time-lapse imagery for classification and applies precise georectification
34 to align ground-based photographs spatially.

35 In this study, we applied this method to quantify *Sasa* expansion into alpine
36 meadows on the western slope of Mt. Tateyama in the northern Japanese Alps.
37 In the nearby Murodo-daira plateau, *Sasa* species (*Sasa kurilensis*, *Sasa spiculosa*,
38 *Sasa senanensis*, and *Sasa palmata*) expanded by 44–260% between 1977 and
39 2015 (Yoshida et al. (2016)). However, prior studies relied on field surveys or
40 manual interpretation of aerial photographs, limiting their spatial coverage. By
41 leveraging automated processing of time-lapse imagery, we produced a large-scale,
42 high-resolution distribution map of *Sasa* across the study area.

43 A key advantage of time-lapse cameras is their capacity to capture frequent, high-
44 resolution records of snowmelt timing—an essential driver of alpine vegetation
45 dynamics. Leveraging this capability, we modeled *Sasa* distributions derived
46 from time-lapse imagery using environmental variables such as snowmelt timing
47 and topographic factors. We then predicted expansion patterns under scenarios
48 of earlier snowmelt. Habitat suitability models (HSMs)—statistical frameworks
49 that relate species occurrence to environmental variables—are widely used to

50 elucidate habitat preferences (Guisan et al. (1998)), guide conservation planning
51 (Larson et al. (2004), Xue et al. (2021)), forecast the spread of invasive species
52 (Gallien et al. (2010), Gallien et al. (2012)), and assess range shifts or extinction
53 risks under climate change (Thomas et al. (2004), Bakkenes et al. (2002), Amagai
54 et al. (2022)).

55 We constructed HSMs using observed *Sasa* distribution and its changes to
56 address two primary questions: (1) whether snowmelt timing serves as a critical
57 determinant of *Sasa* distribution on Mt. Tateyama, and (2) how *Sasa* distribution
58 may shift under future conditions of earlier snowmelt. High-resolution predictions
59 of *Sasa* expansion can substantially support conservation practices by identifying
60 priority areas for *Sasa* removal and improving long-term monitoring strategies.

61 This study provides the first demonstration of detecting and predicting vegeta-
62 tion distribution changes using ground-based time-lapse imagery. Our results
63 demonstrate that time-lapse cameras, with their high temporal frequency and
64 spatial resolution, offer a powerful means for understanding and forecasting
65 vegetation dynamics in alpine ecosystems.

66 2. Materials and Methods

67 Figure 1 presents an overview of the workflow. Using time-lapse imagery
68 from the northern Japanese Alps, we quantified *Sasa* expansion and measured
69 the snowmelt day of year (DOY). *Sasa* expansion was assessed by comparing
70 vegetation classification maps derived from imagery captured in 2012 and 2021,
71 while snowmelt DOY was determined from imagery spanning 2011–2021. Based
72 on the resulting *Sasa* distribution and its changes, together with snowmelt DOY
73 and topographic features derived from a digital elevation model (DEM), we
74 constructed habitat suitability models (HSMs) to predict *Sasa* distribution and
75 expansion. Finally, we incorporated future snowmelt DOY projected from our
76 observations into the HSMs to generate detailed forecasts of future *Sasa* invasion.

77 2.1. Image acquisition

78 To monitor the distribution of *Sasa*, we used images captured by a digital
79 time-lapse camera (EOS 5D MK2, Canon Inc., 21 megapixels) installed by the
80 National Institute for Environmental Studies on the Murodo-sanso mountain
81 lodge (approximately 2,450 m a.s.l.) in the northern Japanese Alps. Since
82 2010, the camera has documented snowmelt and vegetation dynamics on the
83 western slope of Mt. Tateyama (2,350–3,015 m), taking photographs hourly from
84 6:00 to 19:00 between April and November. For details of the installation and
85 operation, see Okamoto et al. (2024). In this study, we used images taken in
86 September–October of 2012 and 2021 for quantifying *Sasa* expansion.

87 A major advantage of time-lapse cameras is their ability to capture fine-scale,
88 daily changes in snow cover. Frequent cloud cover and the steep topography

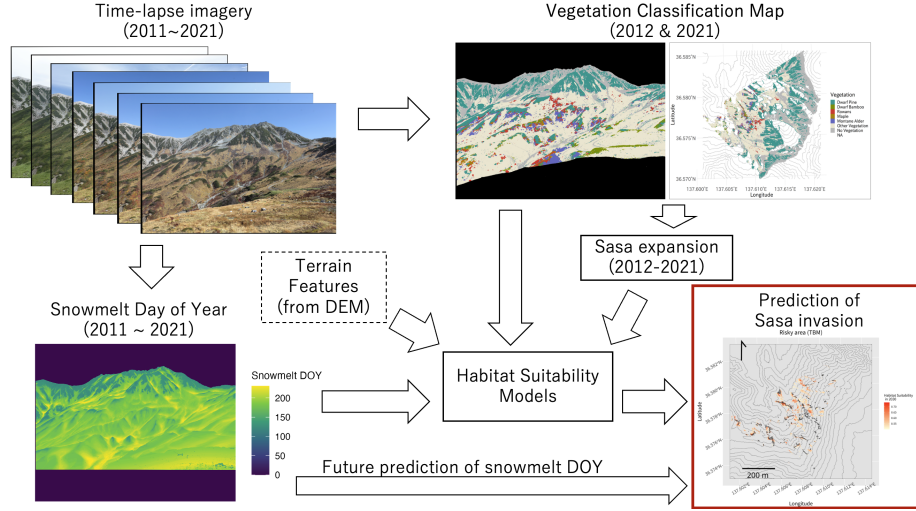


Figure 1: Overview of the proposed method.
We used time-lapse imagery and a DEM for constructing HSMs for predicting the *Sasa* distribution.

of alpine regions often hinder continuous satellite observations, making ground-based time-lapse imagery particularly valuable. Because earlier snowmelt is considered a primary driver of *Sasa* expansion (Kudo et al. (2011)), high-frequency and high-resolution data on snowmelt timing are essential for understanding and predicting its spread. Therefore, we also used imagery acquired from April to August between 2011 and 2021 to calculate the snowmelt day of year (DOY) for each pixel. Snowmelt detection followed a workflow based on Otsu's binarization method (Otsu (1979)) as described in Ide and Oguma (2013). The extracted snowmelt DOYs were subsequently incorporated into the habitat suitability models (HSMs).

2.2. Automated production of vegetation classification maps

Vegetation classification maps were produced using the method developed by Okamoto et al. (2024), which consists of three main steps: image alignment, vegetation classification, and automated georectification.

- **Image alignment:** All images from 2012 and 2021 were aligned to enable precise temporal comparisons. Following Okamoto et al. (2024), we applied a local-feature-based automated alignment approach.
- **Vegetation classification:** Temporal changes in leaf color during autumn were analyzed using a recurrent neural network (RNN), which classified each pixel into seven categories: Dwarf Pine (*Pinus pumila*), Dwarf Bamboo (*Sasa* spp.), Rowans (*Sorbus sambucifolia*, *S. matsumurana*), Maple (*Acer tschonoskii*), Montane Alder (*Alnus viridis* subsp.

112 *maximowiczii*), Other Vegetation (alpine shrubs and herbaceous plants),
113 and No Vegetation.

114

- 115 • **Automated georectification:** We automatically extracted ground
116 control points (GCPs) from existing orthorectified aerial photographs and a
117 digital elevation model (DEM), estimated camera parameters (orientation,
118 focal length, and lens distortion), and transformed the images into georefer-
119 enced data at 1 m spatial resolution using the Python package `alproj`
120 (<https://github.com/Okam/alproj>). The aerial photographs and DEM used
121 for georectification were identical to those in Okamoto et al. (2024).

122 2.3. Quantification of *Sasa* expansion

123 To detect nine-year changes in *Sasa* distribution, we overlaid vegetation classifi-
124 cation maps from 2012 and 2021 (Figure 2). We calculated the area occupied by
125 *Sasa* in each year and quantified its expansion by comparing the two classifica-
126 tion maps. Because *Sasa* can remain beneath shrub canopies, shrub encroachment
127 and growth may cause *Sasa* to become undetectable in time-lapse imagery. Con-
128 sequently, areas that appear to have decreased in *Sasa* cover may not represent
129 true declines. To avoid underestimating expansion due to this limitation, we
130 defined the primary expansion metric as the area of transitions from non-*Sasa*
131 to *Sasa* (i.e., expansion area).

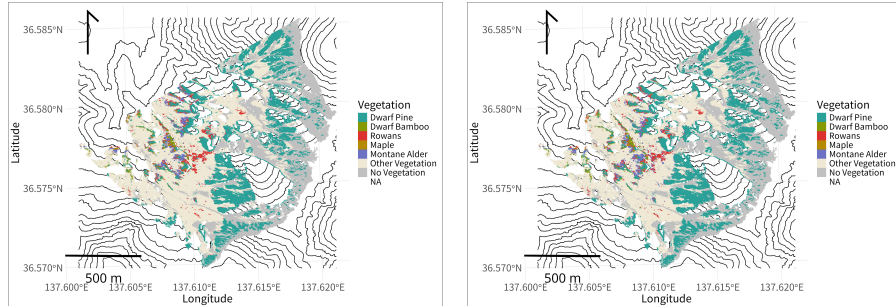


Figure 2: Vegetation classification results for 2012 and 2021.

Vegetation classification maps for 2012 (left) and 2021 (right). *Sasa* expansion was quantified by comparing the spatial extent of its distribution between the two maps.

132 2.4. Habitat suitability modeling

133 To predict future *Sasa* expansion and understand its driver, we constructed
134 habitat suitability models (HSMs). *Sasa* forms complex rhizome systems and
135 extensive clonal networks (Suyama et al. (2000)). While its expansion primarily
136 occurs through rhizome elongation, seed dispersal can also take place after mass
137 or partial flowering events (Miyazaki et al. (2009); Mizuki et al. (2014); Kudo
138 et al. (2011)). As a result, *Sasa* can potentially expand both gradually through
139 rhizome growth and over longer distances through seed dispersal.

To capture these contrasting dispersal processes, we developed two complementary models that predict the *Sasa* distribution observed in 2021 from environmental conditions and the baseline distribution in 2012. The **Topography-Based Model (TBM)** incorporates only topographic variables such as elevation, slope, and snowmelt DOY, representing potential expansion areas assuming that *Sasa* can disperse freely via seeds. In contrast, the **Topography–Distance Model (TDM)** additionally includes the distance from the 2012 *Sasa* distribution as a predictor, constraining the predicted 2021 distribution to areas near existing populations and thus reflecting the limited rhizome-based spread typical of *Sasa*. Comparing the two models allows us to distinguish between the broader potential niche under seed dispersal and the more localized realized expansion expected from clonal growth, providing a realistic range of possible future scenarios.

2.4.1. Explanatory variables

Both models incorporated elevation, slope, aspect, roughness, the Terrain Ruggedness Index (TRI), the Topographic Position Index (TPI), and snowmelt day of year (DOY) as explanatory variables. These topographic features were derived from a 5 m digital elevation model (DEM) provided by the Geospatial Information Authority of Japan and resampled to 1 m resolution to match the vegetation maps.

Snowmelt DOYs were obtained from time-lapse imagery. Although interannual fluctuations were observed, snowmelt timing showed an advancing trend over the past decade. To represent this temporal trend, we fitted a linear regression to per-pixel snowmelt DOYs for each year from 2011 to 2021 and used the predicted 2021 values as explanatory variables in both models. The mean regression coefficient was -0.86 , corresponding to an advance of 8.6 days per decade. For future projections, we extended the same regressions to estimate snowmelt DOYs for 2030 at each pixel. Although some areas obscured by foreground snow cover had uncertain snowmelt dates, these areas showed minimal overlap with the *Sasa* distribution and thus had little impact on our analysis. Additional details on snowmelt timing and its prediction are provided in Section 6. In the TDM, distance from the 2012 *Sasa* distribution was included as an additional explanatory variable to represent dispersal limitation.

2.4.2. Target variable

The TBM was trained to predict the *Sasa* distribution in 2021. Because many *Sasa* patches present in 2012 persisted through 2021, pixels located directly within the 2012 distribution (i.e., at 0 m distance) were excluded from the TDM. Accordingly, the TDM was designed to predict newly colonized locations that appeared between 2012 and 2021.

2.4.3. Data sampling and splitting

2.4.3.1. Data sampling.

Because the *Sasa* distribution is relatively limited compared with other vegetation types (Figure 2), the dataset was imbalanced. To address this, presence

182 data were retained at 1 m resolution, whereas absence data were downsampled
 183 to 5 m resolution to reduce dominance by non-*Sasa* pixels. Additionally, areas
 184 above 2,560 m—where *Sasa* does not occur—were excluded from the analysis.

185 *2.4.3.2. Initial splitting.*

186 To evaluate model performance, we divided the dataset into 80% for training
 187 and 20% for testing. Given the strong spatial autocorrelation among explanatory
 188 variables, we applied spatial block splitting using the R packages **spatialsample**
 189 (Mahoney et al., 2023) and **tidysdm** (Leonardi et al., 2024) to mitigate overfitting
 190 effects (Figure 3, left).

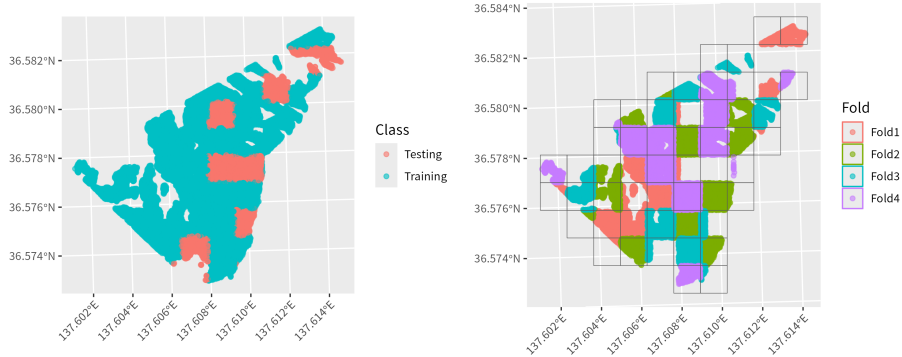


Figure 3: Visualizations of spatial sampling.

The initial split is shown on the left, and the fourfold split used for cross-validation is shown on the right. Spatial sampling was implemented during data splitting to reduce the risk of model overfitting caused by spatial autocorrelation.

191 *2.4.3.3. Cross-validation.*

192 For hyperparameter tuning and ensemble construction, we performed fourfold
 193 cross-validation using the same spatial block splitting approach (Figure 3, right)
 194 on the training dataset.

195 *2.4.4. Model preparation*

196 *2.4.4.1. Model training and evaluation.*

197 We applied four classification algorithms: gradient boosted trees (GBT; Friedman
 198 (2001)), maximum entropy (MaxEnt; Phillips et al. (2006)), random forest
 199 (RF; Breiman (2001)), and generalized additive models (GAM). For all models
 200 except GAM, hyperparameters were tuned via grid search with up to 18 trials.
 201 Model performance was evaluated using the True Skill Statistic (TSS; Allouche
 202 et al. (2006); see Equation 1), which ranges from 0 to 1, with higher values
 203 indicating greater predictive accuracy. (TP), (FP), and (FN) denote the numbers
 204 of true positives, false positives, and false negatives, respectively.

$$\begin{aligned}
recall &= \frac{TP}{TP + FN} \\
specificity &= \frac{TN}{TN + FP} \\
TSS &= recall + specificity - 1
\end{aligned} \tag{1}$$

205 2.4.4.2. *Model ensembling.*

206 We constructed ensemble models using the `blend_predictions` function in
207 the R package `stacks` ([Couch and Kuhn \(2024\)](#)), which estimates blending
208 coefficients via LASSO regularization to maximize cross-validated performance.
209 The ensemble TSS was subsequently evaluated on the independent test dataset.

210 2.4.4.3. *Variable importance computation.*

211 For both the TBM and TDM, variable importance was assessed using permutation
212 loss, defined as the reduction in TSS observed when each explanatory variable
213 was randomly permuted. This measure quantifies the relative contribution of
214 each variable to the overall predictive performance of the model.

215 2.4.5. *Future prediction and definition of risky areas*

216 Using ensemble models built for each of the TBM and TDM, we predicted *Sasa*
217 distribution for 2030 based on the estimated snowmelt DOYs (see Section 2.4.1).
218 In this framework, predictions from the TBM represent areas that could become
219 suitable if *Sasa* disperses via seeds. Under such conditions, *Sasa* is particularly
220 likely to invade low-height alpine grasslands, which correspond to the “Other
221 Vegetation” category in our classification. For conservation purposes, we therefore
222 defined “risky areas” as cells classified as “Other Vegetation” in 2021 whose
223 TBM-predicted habitat suitability (HS) for 2030 exceeded 0.5, and we extracted
224 their spatial distribution accordingly.

225 **3. Results**

226 3.1. *Changes in Sasa distribution between 2012 and 2021*

227 The area occupied by *Sasa* increased from 8,542 m^2 in 2012 to 10,170 m^2 in
228 2021, a net gain of 1,628 m^2 over nine years (+19% relative to 2012). The total
229 expansion area—pixels that transitioned from non-*Sasa* to *Sasa*—amounted to
230 4,095 m^2 (+48% relative to 2012), while the decrease area (from *Sasa* to non-*Sasa*)
231 was 2,467 m^2 . Many of these apparent decreases likely resulted from shrub
232 encroachment and growth. Under such conditions, *Sasa* can persist beneath
233 shrub canopies but becomes undetectable in time-lapse imagery. Therefore, we
234 adopted the expansion area (4,095 m^2) as the primary metric of change. The
235 spatial distribution of expansion is shown in Figure 4. The observed +48%
236 increase over nine years is consistent with previous findings from nearby regions
237 reporting up to +260% expansion over 38 years ([Yoshida et al. \(2016\)](#)).

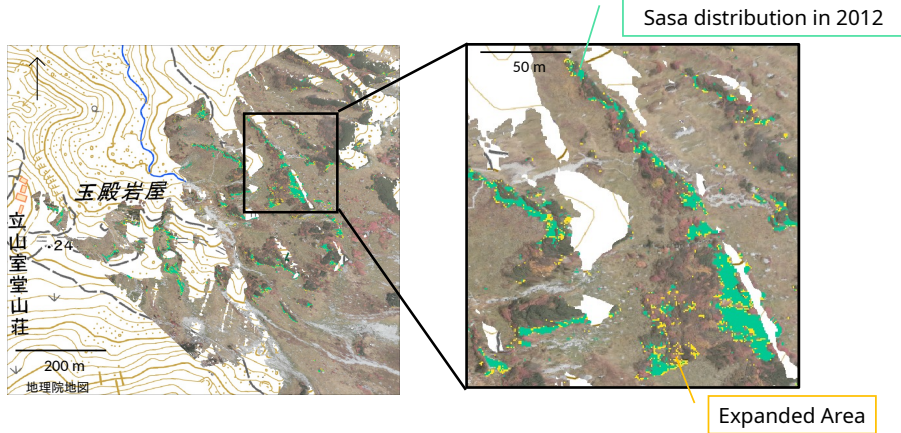


Figure 4: Distribution of *Sasa* expansion between 2012 and 2021. The area occupied by *Sasa* was $8,542 \text{ m}^2$ in 2012 (shown in green) and expanded by $4,095 \text{ m}^2$ (shown in yellow) by 2021, corresponding to a 48% increase relative to 2012.

238 3.2. *HSM performance and variable importance*

239 The TDM consistently achieved higher TSS values than the TBM. Within
240 the TBM, GBT and MaxEnt performed best, while within the TDM, GBT,
241 MaxEnt, and RF outperformed GAM. Ensemble TSS on the test dataset was
242 0.55 for the TBM and 0.70 for the TDM, indicating clear performance gains
243 from incorporating distance in addition to topographic features.

244 Permutation-based variable importance (Figure 6) identified snowmelt DOY
245 as the most influential predictor in the TBM, whereas distance from the 2012
246 *Sasa* distribution was the strongest predictor in the TDM, followed by snowmelt
247 DOY.

248 For the 2021 habitat suitability (HS) maps (Figure 7), the TBM predicted
249 $47,253 \text{ m}^2$ of suitable habitat ($\text{HS} > 0.5$), substantially overestimating the
250 observed distribution ($10,170 \text{ m}^2$). In contrast, the TDM predicted $12,766 \text{ m}^2$,
251 much closer to observations.

252 3.3. *Future prediction and risky areas*

253 From the 2030 HS maps and their differences from 2021 (Figure 8), TBM
254 predicted $27,049 \text{ m}^2$ (57% of the 2021 TBM suitable area) of newly suitable
255 habitat by 2030, while TDM predicted $4,387 \text{ m}^2$ (34%). Conversely, of the areas
256 occupied by *Sasa* in 2021, TBM predicted $2,257 \text{ m}^2$ (21%) to become unsuitable
257 by 2030, and TDM predicted 717 m^2 (7%) to become unsuitable.

258 The spatial distribution of risky areas—cells classified as “Other Vegetation”
259 in 2021 with TBM HS > 0.5 in 2030—is shown in Figure 9.

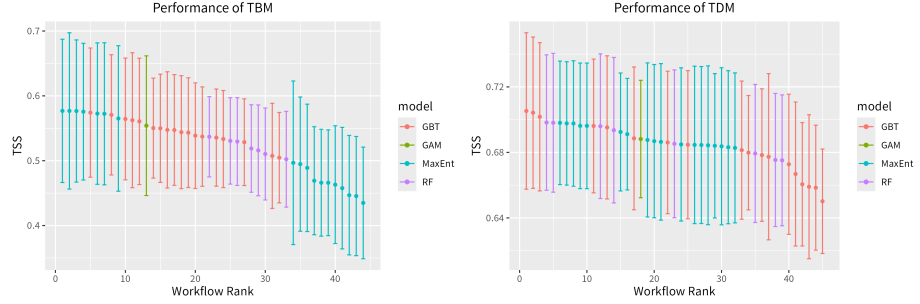


Figure 5: Performance metrics of HSMs obtained through hyperparameter tuning during cross-validation.

TSS scores of HSMs obtained through hyperparameter tuning during cross-validation. The TDM consistently achieved higher TSS values than the TBM, indicating superior predictive performance. Within the TBM framework, GBT and MaxEnt models performed best, whereas within the TDM framework, GBT, MaxEnt, and RF models showed comparably high accuracy.

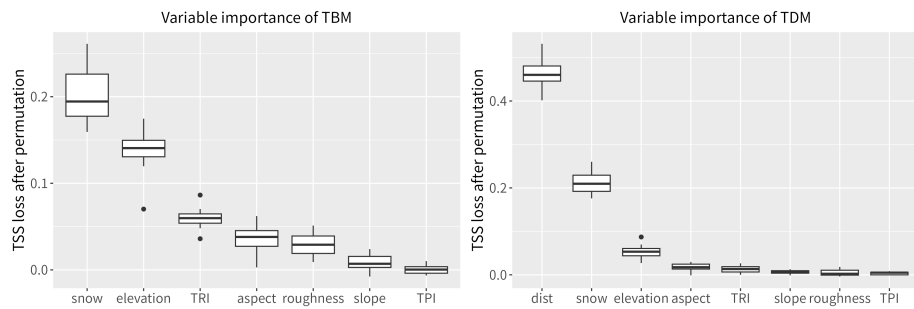


Figure 6: Variable importance for TBM and TDM.

Variable importance based on permutation loss for the TBM and TDM. In the TBM, snowmelt DOY was the most influential variable, whereas in the TDM, distance from the 2012 *Sasa* distribution was the most important, followed by snowmelt DOY.

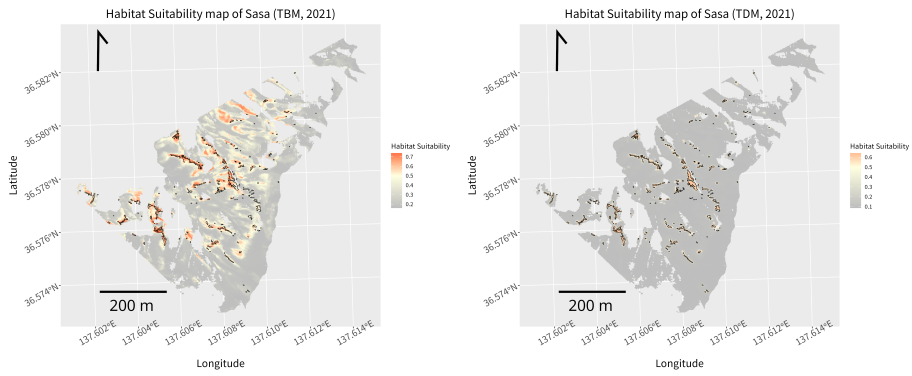


Figure 7: Predicted habitat suitability of *Sasa* in 2021.
 Habitat suitability (HS) maps for 2021 generated by the TBM and TDM. The maps show areas predicted as suitable for *Sasa* habitation ($HS > 0.5$). The TBM predicted $47,253 \text{ m}^2$ as suitable, substantially overestimating the observed distribution of $10,170 \text{ m}^2$. In contrast, the TDM predicted $12,766 \text{ m}^2$, closely matching the observed distribution and demonstrating higher accuracy in reproducing the actual *Sasa* distribution.

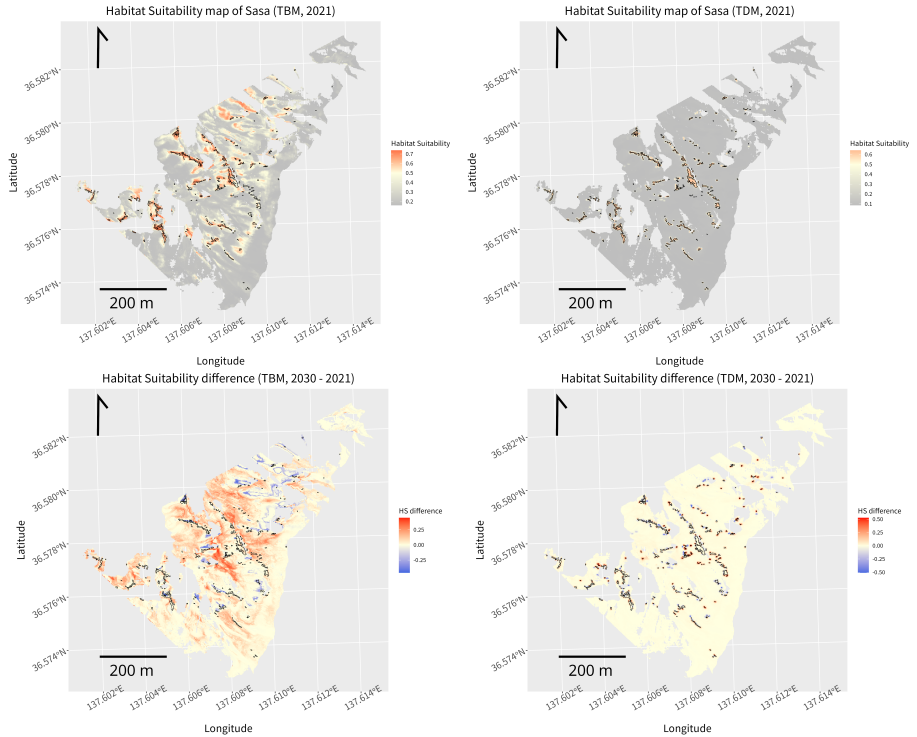


Figure 8: Predicted habitat suitability of Sasa in 2030 and differences from 2021.

Habitat suitability (HS) maps for 2030 and differences from the 2021 HS maps. The TBM predicted $27,049 \text{ m}^2$ (57% of the 2021 suitable area) as newly suitable for Sasa in 2030, while the TDM predicted $4,387 \text{ m}^2$ (34%) as newly suitable. These projections indicate a potential Sasa distribution expansion similar to the past decade. Additionally, even in areas where Sasa was present in 2021, some regions are expected to become unsuitable by 2030. The TBM identifies $2,257 \text{ m}^2$ (21%) as unsuitable, while the TDM identifies 717 m^2 (7%) as unsuitable. These reductions suggest shifts in habitat suitability and Sasa distribution due to earlier snowmelt timing.

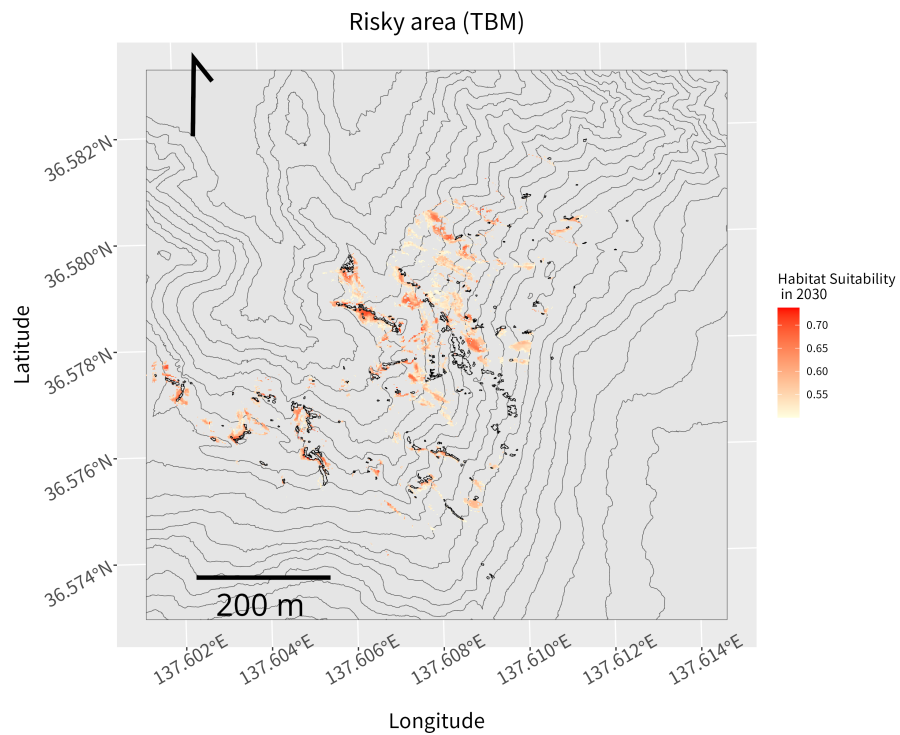


Figure 9: Predicted potential habitats for *Sasa* (risky areas). Potential habitats were extracted from the TBM predictions to support future monitoring and conservation planning. “Risky areas” were defined as cells classified as “Other Vegetation” in 2021 with a predicted 2030 habitat suitability (HS) greater than 0.5.

260 **4. Discussion**

261 In this study, we applied the method proposed in our previous work to quantify
262 the expansion of *Sasa* distribution in the northern Japanese Alps using
263 time-lapse camera imagery. By integrating these data into habitat suitability
264 models (HSMs), we successfully assessed the future risk of *Sasa* expansion at an
265 exceptionally high spatial resolution of 1 m.

266 The upward expansion of competitively dominant species such as *Sasa* poses
267 a serious threat to the conservation of alpine vegetation. The findings of this
268 study provide a critical foundation for prioritizing conservation actions and
269 designing long-term monitoring strategies. In the following section, we discuss
270 the advantages of the proposed workflow for understanding and conserving alpine
271 vegetation, as well as its methodological limitations and future applications.

272 *4.1. Expansion of Sasa and its drivers*

273 Comparison of vegetation classification maps from 2012 and 2021 enabled us to
274 spatially identify areas of *Sasa* expansion. Incorporating HSMs further allowed
275 us to investigate the environmental factors driving this expansion. Variable
276 importance analyses for both the TBM and TDM (Figure 6) indicated that
277 snowmelt DOY was a major determinant. Moreover, predictions for 2030,
278 assuming earlier snowmelt than in 2021, suggested continued *Sasa* expansion.
279 These results indicate that earlier snowmelt has facilitated *Sasa* expansion,
280 consistent with previous findings (Kudo et al. (2011)) that link earlier snowmelt
281 to increased soil dryness and extended growing periods that favor *Sasa* growth.

282 At the same time, the TBM substantially overestimated *Sasa* distribution in
283 2021. Although adding distance as an explanatory variable improved model
284 accuracy, at least two interpretations of the overestimation are possible. First,
285 areas predicted as suitable by the TBM may indeed be habitable, but *Sasa* has not
286 yet colonized them due to its limited dispersal capacity. In fact, no isolated *Sasa*
287 patches formed by seed dispersal were observed in the expansion areas between
288 2012 and 2021, supporting the idea that low dispersal ability creates a large gap
289 between potential and realized niches. Second, the overestimation may reflect
290 missing explanatory variables. In this case, *Sasa* generally occupies its potential
291 niche, but the TBM overestimated distribution because it failed to incorporate
292 important environmental factors. The improved accuracy of the TDM could then
293 be explained by a strong spatial correlation between the 2012 distribution and
294 such unmeasured variables. Soil structure or soil moisture, for instance, could play
295 this role. To distinguish between these interpretations, the TBM should ideally be
296 extended to include additional environmental predictors, although obtaining such
297 comprehensive datasets remains challenging. Alternatively, process-based models
298 that simulate dispersal dynamics could help clarify whether the overestimation
299 results from dispersal limitations or omitted environmental factors.

300 *4.2. Future prediction and potential applications*

301 This study demonstrated that combining time-lapse cameras with HSMs en-
302 ables exceptionally fine-scale (1 m) prediction of future vegetation distributions.

303 The integration of time-lapse imagery and HSMs is unprecedented. In contrast,
304 conventional species distribution models typically operate at much coarser reso-
305 lutions (e.g., 1 km), as future climate projections are generally available only at
306 coarse spatial scales (e.g., alpine vegetation studies: [Amagai et al. \(2022\)](#)). Here,
307 by directly observing snowmelt timing—a key determinant of *Sasa* distribution—
308 using time-lapse cameras, we achieved high-resolution predictions. Because
309 snowmelt timing requires both frequent and spatially extensive monitoring,
310 time-lapse cameras are particularly suited for this purpose.

311 High-resolution predictions are especially valuable for designing practical conser-
312 vation strategies, such as identifying priority areas for *Sasa* removal or selecting
313 effective monitoring sites. For example, a prediction at 1 km resolution might
314 suggest that an entire square kilometer is at risk, which would be unrealistic for
315 management. In contrast, predictions at 1 m resolution enable more targeted
316 and efficient conservation planning.

317 In this study, we predicted future snowmelt timing using a simple linear
318 regression based on a decade of past data. While this approach provided a useful
319 proof of concept, it does not represent a realistic long-term forecast. In the alpine
320 regions, strong seasonal winds and complex topography cause substantial snow
321 redistribution, making snowmelt prediction a continuing challenge. Therefore,
322 we did not attempt to refine future snowmelt predictions here. However, as high-
323 resolution climate projections become available, the accuracy of *Sasa* distribution
324 forecasts will also improve. The future expansion presented here should thus be
325 interpreted not as a literal forecast but as a scenario based on the assumption
326 of continued earlier snowmelt—an assumption that should be re-evaluated as
327 understanding of alpine snow processes advances.

328 5. Conclusion

329 This study demonstrated the effectiveness of integrating time-lapse cameras with
330 habitat suitability models (HSMs) to detect and predict changes in vegetation
331 distribution at 1 m resolution. Focusing on the expansion of *Sasa* in the northern
332 Japanese Alps, we quantified its distributional changes over the past nine years
333 and identified earlier snowmelt as a major driver of its spread. Furthermore,
334 our projections indicate that *Sasa* expansion is likely to continue in the coming
335 decades.

336 The expansion of *Sasa* poses a serious threat to alpine plant diversity, and the
337 framework developed here provides direct applications for conservation planning.
338 Predictions at 1 m resolution offer practical guidance for selecting monitoring
339 sites and prioritizing areas for *Sasa* removal, enabling more efficient allocation
340 of conservation resources. Beyond *Sasa*, this approach can be extended to other
341 invasive species, as well as to plant communities highly sensitive to climate change,
342 demonstrating broad potential for use in alpine regions and other vulnerable
343 ecosystems worldwide.

³⁴⁴ In summary, this study highlights the power of combining high-frequency time-
³⁴⁵ lapse observations with HSM-based modeling to advance the understanding and
³⁴⁶ prediction of vegetation dynamics. This integrated framework refines climate
³⁴⁷ impact assessment in alpine ecosystems and supports the development of practical,
³⁴⁸ conservation-oriented ecology.

³⁴⁹ **6. Supplementary Information**

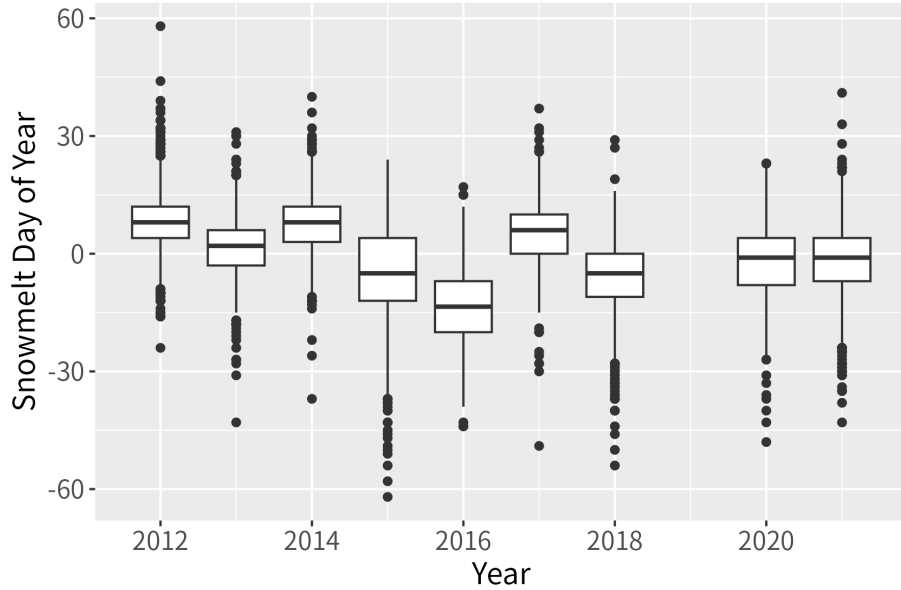


Fig. S1: Decadal trend in snowmelt timing (2011–2021).
Changes in snowmelt Day of Year (DOY) relative to 2011 (set as 0). A total of 1,000 pixels were randomly sampled and plotted. Despite large interannual fluctuations, an overall trend toward earlier snowmelt is suggested. Data for 2019 are missing due to construction work at the mountain lodge where the camera was installed.

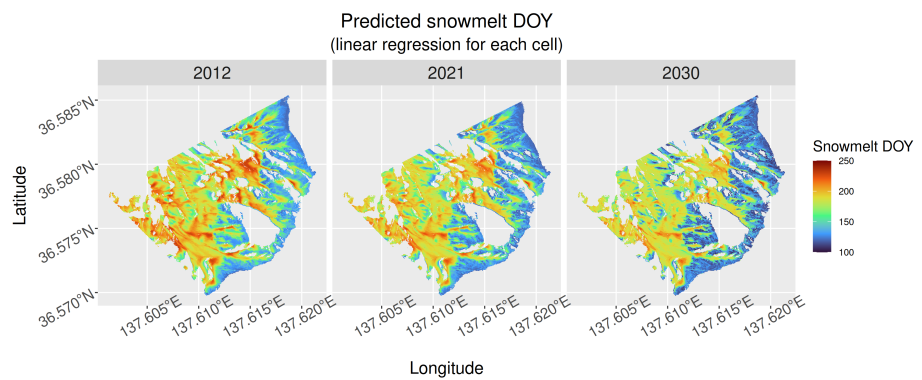


Fig. S2: Predicted snowmelt DOY (linear regression for each cell).
Predicted snowmelt DOY for 2012, 2021, and 2030, derived from cell-wise linear regression models fitted to annual snowmelt DOY between 2011 and 2021.

Changes in predicted snowmelt DOY
(2021-2012; negative values indicate earlier snowmelt)

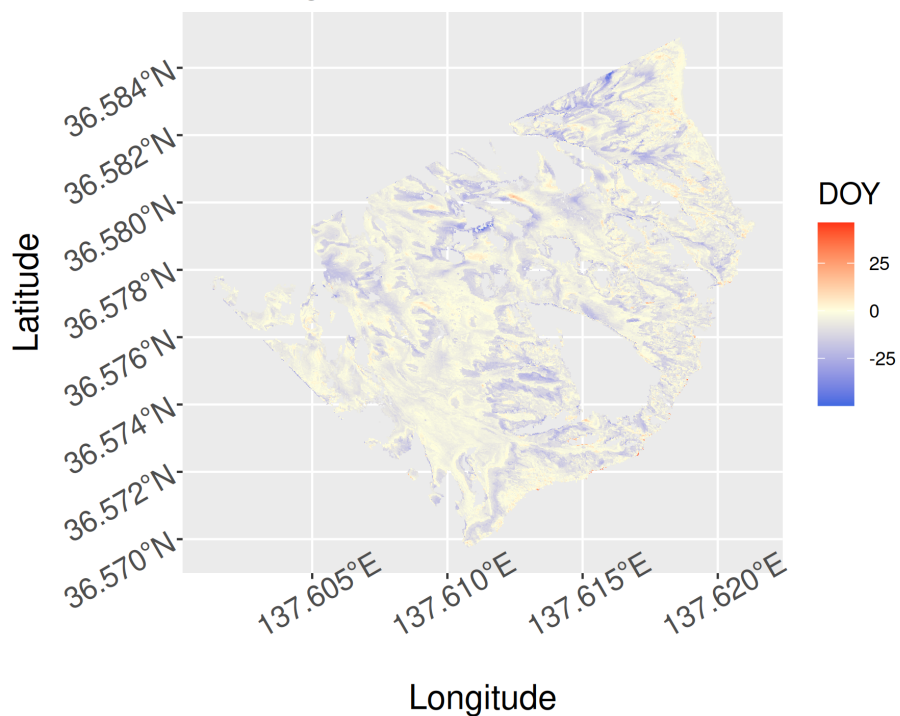


Fig. S3: Changes in predicted snowmelt DOY (2021 – 2012; negative values indicate earlier snowmelt).

Difference in predicted snowmelt DOY between 2012 and 2021. Most areas show earlier snowmelt, with clear spatial heterogeneity in the degree of change.

350 **References**

- 351 Allouche, O., Tsoar, A., Kadmon, R., 2006. Assessing the accuracy of
352 species distribution models: prevalence, kappa and the true skill statistic
353 (tss). Journal of Applied Ecology 43, 1223–1232. URL: <https://onlinelibrary.wiley.com/doi/full/10.1111/j.1365-2664.2006.01214.x>
354 <https://onlinelibrary.wiley.com/doi/abs/10.1111/j.1365-2664.2006.01214.x>
355 <https://besjournals.onlinelibrary.wiley.com/doi/10.1111/j.1365-2664.2006.01214.x>,
356 doi:[10.1111/J.1365-2664.2006.01214.X](https://doi.org/10.1111/J.1365-2664.2006.01214.X).
- 358 Amagai, Y., Oguma, H., Ishihama, F., 2022. Predicted scarcity of
359 suitable habitat for alpine plant communities in northern japan
360 under climate change. Applied Vegetation Science , e12694URL:
361 <https://onlinelibrary.wiley.com/doi/full/10.1111/avsc.12694>
362 <https://onlinelibrary.wiley.com/doi/abs/10.1111/avsc.12694>
363 doi:[10.1111/AVSC.12694](https://doi.org/10.1111/AVSC.12694).
- 364 Bakkenes, M., Alkemade, J.R., Ihle, F., Leemans, R., Latour, J.B., 2002.
365 Assessing effects of forecasted climate change on the diversity and dis-
366 tribution of european higher plants for 2050. Global Change Biology 8,
367 390–407. URL: <https://onlinelibrary.wiley.com/doi/full/10.1046/j.1354-1013.2001.00467.x>
368 <https://onlinelibrary.wiley.com/doi/abs/10.1046/j.1354-1013.2001.00467.x>,
369 doi:[10.1046/J.1354-1013.2001.00467.X](https://doi.org/10.1046/J.1354-1013.2001.00467.X).
- 371 Breiman, L., 2001. Random forests. Machine Learning 45, 5–32. URL:
372 <https://link.springer.com/article/10.1023/A:1010933404324>, doi:[10.1023/A:1010933404324/METRICS](https://doi.org/10.1023/A:1010933404324).
- 374 Couch, S., Kuhn, M., 2024. Tidy model stacking [r package stacks version 1.0.5].
375 CRAN: Contributed Packages URL: <https://CRAN.R-project.org/package=stacks>, doi:[10.32614/CRAN.PACKAGE.STACKS](https://doi.org/10.32614/CRAN.PACKAGE.STACKS).
- 377 Dullinger, S., Dirnböck, T., Grabherr, G., 2003. Patterns of shrub invasion into
378 high mountain grasslands of the northern calcareous alps, austria. Arctic,
379 Antarctic, and Alpine Research 35, 434–441. URL: <http://www.jstor.org/stable/1552344>.
- 381 Friedman, J.H., 2001. Greedy function approximation: A gradient boosting
382 machine. The Annals of Statistics 29, 1189–1232. URL: <https://doi.org/10.1214/aos/1013203451>, doi:[10.1214/aos/1013203451](https://doi.org/10.1214/aos/1013203451).
- 384 Gallien, L., Douzet, R., Pratte, S., Zimmermann, N.E., Thuiller, W., 2012.
385 Invasive species distribution models – how violating the equilibrium assumption
386 can create new insights. Global Ecology and Biogeography 21, 1126–1136.
387 URL: <https://doi.org/10.1111/j.1466-8238.2012.00768.x>, doi:<https://doi.org/10.1111/j.1466-8238.2012.00768.x>.

- 389 Gallien, L., Münkemüller, T., Albert, C.H., Boulangeat, I., Thuiller, W.,
390 2010. Predicting potential distributions of invasive species: where to
391 go from here? *Diversity and Distributions* 16, 331–342. URL: <https://onlinelibrary.wiley.com/doi/full/10.1111/j.1472-4642.2010.00652.x>
392 <https://onlinelibrary.wiley.com/doi/abs/10.1111/j.1472-4642.2010.00652.x>
393 <https://onlinelibrary.wiley.com/doi/10.1111/j.1472-4642.2010.00652.x>,
394 doi:[10.1111/j.1472-4642.2010.00652.X](https://doi.org/10.1111/j.1472-4642.2010.00652.x).
- 395
- 396 Gottfried, M., Pauli, H., Futschik, A., Akhalkatsi, M., Barančok, P., Alonso,
397 J.L.B., Coldea, G., Dick, J., Erschbamer, B., Calzado, M.R.F., Kazakis, G.,
398 Krajčí, J., Larsson, P., Mallaun, M., Michelsen, O., Moiseev, D., Moiseev, P.,
399 Molau, U., Merzouki, A., Nagy, L., Nakhutsrishvili, G., Pedersen, B., Pelino,
400 G., Puscas, M., Rossi, G., Stanisci, A., Theurillat, J.P., Tomaselli, M., Villar,
401 L., Vittoz, P., Vogiatzakis, I., Grabherr, G., 2012. Continent-wide response of
402 mountain vegetation to climate change. *Nature Climate Change* 2, 111–115.
403 URL: www.nature.com/natureclimatechange, doi:[10.1038/nclimate1329](https://doi.org/10.1038/nclimate1329).
- 404
- 405 Grabherr, G., 2003. Alpine Vegetation Dynamics and Climate Change - a
406 Synthesis of Long-Term Studies and Observations. Springer Berlin Heidelberg.
407 pp. 399–409. URL: https://doi.org/10.1007/978-3-642-18967-8_24, doi:[10.1007/978-3-642-18967-8_24](https://doi.org/10.1007/978-3-642-18967-8_24).
- 408
- 409 Grabherr, G., Gottfried, M., Pauli, H., 2010. Climate change impacts in
410 alpine environments. *Geography Compass* 4, 1133–1153. URL: <https://onlinelibrary.wiley.com/doi/full/10.1111/j.1749-8198.2010.00356.x>
411 <https://onlinelibrary.wiley.com/doi/abs/10.1111/j.1749-8198.2010.00356.x>
412 <https://compass.onlinelibrary.wiley.com/doi/10.1111/j.1749-8198.2010.00356.x>,
413 doi:[10.1111/j.1749-8198.2010.00356.X](https://doi.org/10.1111/j.1749-8198.2010.00356.x).
- 414
- 415 Guisan, A., Theurillat, J., Kienast, F., 1998. Predicting the potential distribution
416 of plant species in an alpine environment. *Journal of Vegetation Science* 9,
65–74. doi:[10.2307/3237224](https://doi.org/10.2307/3237224).
- 417
- 418 Hock, R., Rasul, G., Adler, C., Ca;ceres, B., Gruber, S., Hirabayashi, Y., Jackson,
419 M., Kääb, A., Kang, S., Kutuzov, S., Milner, A., Molau, U., Morin, S., Orlove,
420 B., Steltzer, H., Allen, S., Arenson, L., Banerjee, S., Barr, I., Bórquez, R.,
421 Brown, L., Cao, B., Carey, M., Cogley, G., Fischlin, A., de Sherbinin, A.,
422 Eckert, N., Geertsema, M., Hagenstad, M., Honsberg, M., Hood, E., Huss,
423 M., Zamora, E.J., Kotlarski, S., Lefevre, P.M., Moreno, J.I.L., Lundquist,
424 J., McDowell, G., Mills, S., Mou, C., Nepal, S., Noetzli, J., Palazzi, E.,
425 Pepin, N., Rixen, C., Shahgedanova, M., Skiles, S.M., Vincent, C., Viviroli,
426 D., Weyhenmeyer, G.A., Sherpa, P.Y., Weyer, N., Wouters, B., Yasunari,
427 T., You, Q., Zhang, Y., 2019. High Mountain Areas. Cambridge University
428 Press. pp. 131–202. URL: <https://www.ipcc.ch/srocc/chapter/chapter-2/>,
doi:[10.1017/9781009157964.004](https://doi.org/10.1017/9781009157964.004).
- 429
- 430 Ide, R., Oguma, H., 2013. A cost-effective monitoring method using digital
time-lapse cameras for detecting temporal and spatial variations of snowmelt

- 431 and vegetation phenology in alpine ecosystems. Ecological Informatics 16,
432 25–34. URL: [https://doi.org/10.1016/j.
433 ECOINF.2013.04.003](https://doi.org/10.1016/j.ecoinf.2013.04.003).
- 434 Klanderud, K., 2005. Climate change effects on species interactions in an
435 alpine plant community. Journal of Ecology 93, 127–137. URL: [https://
436 //onlinelibrary.wiley.com/doi/full/10.1111/j.1365-2745.2004.00944.x](https://onlinelibrary.wiley.com/doi/full/10.1111/j.1365-2745.2004.00944.x)
437 [https://
438 //besjournals.onlinelibrary.wiley.com/doi/10.1111/j.1365-2745.2004.00944.x](https://onlinelibrary.wiley.com/doi/abs/10.1111/j.1365-2745.2004.00944.x),
439 doi:[10.1111/j.1365-2745.2004.00944.X](https://doi.org/10.1111/j.1365-2745.2004.00944.X).
- 440 Kudo, G., Amagai, Y., Hoshino, B., Kaneko, M., 2011. Invasion of
441 dwarf bamboo into alpine snow-meadows in northern japan: pattern of
442 expansion and impact on species diversity. Ecology and Evolution 1,
443 85–96. URL: [https://
444 //onlinelibrary.wiley.com/doi/abs/10.1002/ece3.9](https://onlinelibrary.wiley.com/doi/full/10.1002/ece3.9)[https://onlinelibrary.wiley.com/doi/10.1002/ece3.9](https://onlinelibrary.wiley.
445 com/doi/10.1002/ece3.9), doi:[10.1002/ECE3.9](https://doi.org/10.1002/ECE3.9).
- 446 Kudo, G., Kawai, Y., Amagai, Y., Winkler, D.E., 2017. Degradation and recovery
447 of an alpine plant community: experimental removal of an encroaching dwarf
448 bamboo. Alpine Botany 127, 75–83. URL: [https://link.springer.com/article/
10.1007/s00035-016-0178-2](https://link.springer.com/article/
449 10.1007/s00035-016-0178-2), doi:[10.1007/S00035-016-0178-2](https://doi.org/10.1007/S00035-016-0178-2).
- 450 Larson, M.A., Thompson, F.R., Millspaugh, J.J., Dijak, W.D., Shifley, S.R., 2004.
451 Linking population viability, habitat suitability, and landscape simulation
452 models for conservation planning. Ecological Modelling 180, 103–118. doi:[10.1016/J.ECOLMODEL.2003.12.054](https://doi.org/10.1016/J.ECOLMODEL.2003.12.054).
- 453 Leonardi, M., Colucci, M., Pozzi, A.V., Scerri, E.M., Manica, A., 2024.
454 tidysdm: Leveraging the flexibility of tidymodels for species distribution
455 modelling in r. Methods in Ecology and Evolution 15, 1789–1795. URL:
456 [https://
457 //onlinelibrary.wiley.com/doi/abs/10.1111/2041-210X.14406](https://onlinelibrary.wiley.com/doi/full/10.1111/2041-210X.14406)[https://
459 //besjournals.onlinelibrary.wiley.com/doi/10.1111/2041-210X.14406](https://
458 //besjournals.onlinelibrary.wiley.com/doi/10.1111/2041-210X.14406),
460 doi:[10.1111/2041-210X.14406](https://doi.org/10.1111/2041-210X.14406).
- 461 Mahoney, M.J., Johnson, L.K., Silge, J., Frick, H., Kuhn, M., Beier, C.M., 2023.
462 Assessing the performance of spatial cross-validation approaches for models of
463 spatially structured data URL: <https://arxiv.org/abs/2303.07334v1>.
- 464 Miyazaki, Y., Ohnishi, N., Takafumi, H., Hiura, T., 2009. Genets of dwarf
465 bamboo do not die after one flowering event: Evidence from genetic structure
466 and flowering pattern. Journal of Plant Research 122, 523–528. URL: [https://
468 //link.springer.com/article/10.1007/s10265-009-0241-9](https://
467 //link.springer.com/article/10.1007/s10265-009-0241-9), doi:[10.1007/S10265-009-0241-9/TABLES/1](https://doi.org/10.1007/S10265-
009-0241-9/TABLES/1).
- 469 Mizuki, I., Sato, A., Matsuo, A., Suyama, Y., Suzuki, J.I., Makita, A., 2014.
470 Clonal structure, seed set, and self-pollination rate in mass-flowering bamboo
471 species during off-year flowering events. PLOS ONE 9, e105051. URL: [https://doi.org/10.1371/journal.pone.0105051](https://
472 //doi.org/10.1371/journal.pone.0105051).

- 472 [//journals.plos.org/plosone/article?id=10.1371/journal.pone.0105051](https://journals.plos.org/plosone/article?id=10.1371/journal.pone.0105051), doi:[10.1371/JOURNAL.PONE.0105051](#).
- 473
- 474 Okamoto, R., Ide, R., Oguma, H., 2024. Automatically drawing veg-
475 etation classification maps using digital time-lapse cameras in alpine
476 ecosystems. *Remote Sensing in Ecology and Conservation* 10, 188–202.
477 URL: <https://onlinelibrary.wiley.com/doi/full/10.1002/rse2.364><https://onlinelibrary.wiley.com/doi/abs/10.1002/rse2.364><https://zslpublications.onlinelibrary.wiley.com/doi/10.1002/rse2.364>, doi:[10.1002/RSE2.364](#).
- 475
- 480 Otsu, N., 1979. A threshold selection method from gray-level histograms. *IEEE
481 Trans Syst Man Cybern SMC-9*, 62–66. doi:[10.1109/TSMC.1979.4310076](#).
- 482
- 483 Phillips, S.B., Aneja, V.P., Kang, D., Arya, S.P., 2006. Maximum entropy mod-
484 eling of species geographic distributions. *Ecological Modelling* 190, 231–259.
485 doi:[10.1016/J.ECOLMODEL.2005.03.026](#).
- 486
- 487 Suyama, Y., Obayashi, K., Hayashi, I., 2000. Clonal structure in a
488 dwarf bamboo (*sasa senanensis*) population inferred from amplified
489 fragment length polymorphism (aflp) fingerprints. *Molecular Ecology* 9,
490 901–906. URL: <https://onlinelibrary.wiley.com/doi/full/10.1046/j.1365-294x.2000.00943.x><https://onlinelibrary.wiley.com/doi/abs/10.1046/j.1365-294x.2000.00943.x>, doi:[10.1046/J.1365-294X.2000.00943.X](#).
- 491
- 492 Thomas, C.D., Cameron, A., Green, R.E., Bakkenes, M., Beaumont, L.J.,
493 Collingham, Y.C., Erasmus, B.F., Siqueira, M.F.D., Grainger, A., Hannah,
494 L., Hughes, L., Huntley, B., Jaarsveld, A.S.V., Midgley, G.F., Miles, L.,
495 Ortega-Huerta, M.A., Peterson, A.T., Phillips, O.L., Williams, S.E., 2004.
496 Extinction risk from climate change. *Nature* 2003 427:6970 427, 145–148. URL:
497 <https://www.nature.com/articles/nature02121>, doi:[10.1038/nature02121](#).
- 498
- 499 Xue, T., Gadagkar, S.R., Albright, T.P., Yang, X., Li, J., Xia, C., Wu, J., Yu, S.,
500 2021. Prioritizing conservation of biodiversity in an alpine region: Distribution
501 pattern and conservation status of seed plants in the qinghai-tibetan plateau.
502 *Global Ecology and Conservation* 32, e01885. doi:[10.1016/J.GECCO.2021.E01885](#).
- 503
- 504 Yoshida, M., Takahashi, K., Ohmiya, T., 2016. Expansion of dwarf bamboo
505 communities in murodo-daira, tateyama mountains, as revealed by aerial
506 photography. *Bulletin of the Botanic Gardens of Toyama* , 9–17.